Title

Visualization of an axion insulating state at the transition between 2 chiral quantum anomalous Hall states

Journal

Proceedings of the National Academy of Sciences of the United States of America, 116(29)

ISSN

0027-8424

Authors

Allen, Monica
Cui, Yongtao
Yue, Eric
et al.

Publication Date

2019-07-16

DOI

10.1073/pnas.1818255116

Peer reviewed

Visualization of an axion insulating state at the transition between 2 chiral quantum anomalous Hall states

Monica Allen[a,b], Yongtao Cui[c], Eric Yue Ma[a], Masataka Mogi[d], Minoru Kawamura[e], Ion Cosma Fulga[f], David Goldhaber-Gordon[b,g,h], Yoshinori Tokura[d,e], and Zhi-Xun Shen[a,b,h,1]

[a]Department of Applied Physics, Stanford University, Stanford, CA 94305; [b]Geballe Laboratory for Advanced Materials, Stanford University, Stanford, CA 94305; [c]Department of Physics, University of California, Riverside, CA 92521; [d]Department of Applied Physics, University of Tokyo, Tokyo 113-8654, Japan; [e]Strong Correlation Physics Research Group, RIKEN Center for Emergent Matter Science, Saitama 351-0198, Japan; [f]Institute for Theoretical Solid State Physics, The Leibniz Institute for Solid State and Materials Research Dresden, 01069 Dresden, Germany; [g]Department of Physics, Stanford University, Stanford, CA 94305; and [h]Stanford Institute for Materials and Energy Sciences, Stanford Linear Accelerator Center National Accelerator Laboratory, Menlo Park, CA 94025

Edited by Weida Wu, Rutgers University, Piscataway, NJ, and accepted by Editorial Board Member Angel Rubio June 11, 2019 (received for review November 7, 2018)

Quantum-relativistic materials often host electronic phenomena with exotic spatial distributions. In particular, quantum anomalous Hall (QAH) insulators feature topological boundary currents whose chirality is determined by the magnetization orientation. However, understanding the microscopic nature of edge vs. bulk currents has remained a challenge due to the emergence of multidomain states at the phase transitions. Here we use microwave impedance microscopy (MIM) to directly image chiral edge currents and phase transitions in a magnetic topological insulator. Our images reveal a dramatic change in the edge state structure and an unexpected microwave response at the topological phase transition between the Chern number $N = 1$ and $N = -1$ states, consistent with the emergence of an insulating $N = 0$ state. The magnetic transition width is independent of film thickness, but the transition pattern is distinct in differently initiated field sweeps. This behavior suggests that the $N = 0$ state has 2 surface states with Hall conductivities of $\frac{1}{2}e^2/h$ but with opposite signs.

topological states of matter | quantum anomalous Hall systems | microwave impedance microscopy

The experimental discovery of the quantum anomalous Hall (QAH) effect is a major advance in condensed-matter physics (1–8). This discovery followed a string of theoretical developments (9–13). The QAH insulator is a state of matter characterized by a chiral 1D edge current that encloses an insulating bulk. This state, which persists in the absence of a magnetic field, can be realized in a thin slab of a 3D topological insulator by introducing magnetic dopants that break time-reversal symmetry and open a mass gap in the Dirac surface states (14). Applying an external magnetic field induces a quantum phase transition between 2 topologically distinct states corresponding to up and down magnetization orientations, which are labeled with the Chern numbers $N = \pm 1$ (1, 2, 4, 8, 12).

In magnetic heterostructures, in which magnetic ions are introduced only near top and bottom surfaces of the topological insulator, a richer picture emerges because the magnetizations near the upper and lower surface states can be tuned independently, allowing access to an expanded family of topological phases. When the upper and lower magnetizations point in opposite directions, theory predicts the emergence of a new topologically nontrivial state, known as the axion insulator, that should feature a quantized plateau at zero Hall conductivity at the transition between the $N = \pm 1$ states (8, 15–19). In the axion state, the upper and lower surface states should contribute a half-quantized Hall conductance of opposite sign, $\pm 1/2\ e^2/h$, together resulting in uniformly insulating behavior. This contrasts with the electronic nature of the $N = \pm 1$ states, in which the surface conductivities add to a quantized value $\sigma_{xy} = \pm 1\ e^2/h$.

However, elucidating the local electronic structure of the phase transition and existence of the axion state using transport techniques is complicated by the emergence of multidomain states (7, 12, 19, 20) and theoretically predicted band crossings (10, 11) at the phase transitions. Furthermore, reaching the axion insulator state likely requires making the film thick enough to suppress the hybridization gap, which could also be thick enough to allow enhanced sidewall conduction. These features motivate use of imaging techniques to provide a comprehensive spatial map of states across the full phase diagram to avoid some of the ambiguities of the transport data interpretation.

Results

Microwave Imaging of Chiral Edge Modes in a Magnetic Topological Insulator. Here we provide a real-space visualization of the local conductivity profile in Cr modulation doped $(Bi,Sb)_2Te_3$

Significance

Magnetic topological insulators host chiral dissipationless edge modes, which mimic quantum Hall states but persist in the absence of a magnetic field. We use microwave impedance microscopy, which characterizes the local complex conductivity of a material, to provide direct visualization of these edge states and monitor their evolution across a magnetic-field–induced phase transition. The resulting images reveal an insulating state, which exhibits a distinct geometry of current flow, at the boundary between 2 quantum anomalous Hall (QAH) states with opposite chirality. Due to their immunity to backscattering, the edge currents present in the QAH regime provide a promising platform for future investigations of chiral Majorana modes, key building blocks for a topological quantum computer.

Author contributions: M.A., D.G.-G., Y.T., and Z.-X.S. designed research; M.A., Y.C., E.Y.M., M.M., M.K., Y.T., and Z.-X.S. performed research; I.C.F. contributed new reagents/analytic tools; M.A., I.C.F., and D.G.-G. analyzed transport data; and M.A., D.G.-G., and Z.-X.S. wrote the paper.

Conflict of interest statement: Z.-X.S. is a cofounder of PrimeNano Inc., which licensed the sMIM technology from Stanford University for commercial instruments. This technology was modified for low-temperature measurement in this report.

This article is a PNAS Direct Submission. W.W. is a guest editor invited by the Editorial Board.

[1]To whom correspondence may be addressed. Email: zxshen@stanford.edu.

This article contains supporting information online at www.pnas.org/lookup/suppl/doi:10.1073/pnas.1818255116/-/DCSupplemental.

Published online July 2, 2019.

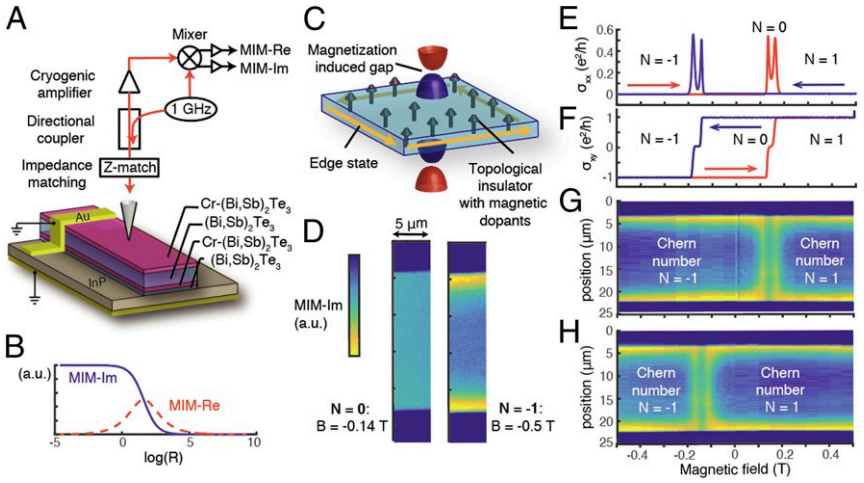

Fig. 1. Imaging edge states in a magnetic topological insulator. (*A*) Schematic of MIM on a Cr-modulation doped topological insulator. (*B*) The real (red) and imaginary (blue) parts of the microwave response curves exhibit a sharp dependence on the local sample resistivity *R*. (*C*) Schematic of the QAH effect in a 3D topological insulator. Magnetic dopants open a gap in the surface Dirac cones, giving rise to chiral edge currents. (*D*, *Right*) Real-space map of the imaginary microwave response in the QAH regime shows enhanced signal at the sample edges. (*D*, *Left*) Real-space image in the $N = 0$ state depicts uniformly insulating behavior. (*E* and *F*) Transport measurements showing quantization of the Hall conductivity and magnetic hysteresis with sweep direction. (*G* and *H*) Real-space maps of the local conductivity (MIM-Im), illustrating the microscopic evolution of the edge state structure across phase transitions between topologically distinct states.

using microwave impedance microscopy (MIM) at a temperature of 450 mK. The sample is a 3D topological insulator whose upper and lower surface states couple separately to a pair of magnetic dopant layers with different coercive fields (Fig. 1*A*) (17, 21). Microwaves at a frequency of 1 GHz are sent to the tip via an impedance matching network, and the amplitudes of the reflected signals that are in and out of phase with excitation are recorded. The complex microwave response, which can be quantified in the theoretical curves presented in Fig. 1*B*, provides a local measurement of dissipation and screening in response to high-frequency electromagnetic fields from the tip (22, 23).

By tracking the evolution of the microwave response in the magnetic field, we construct a phase diagram of competing topological states and unveil the microscopic nature of dissipation and conductivity in each phase. Well-defined edge excitations appear in the quantum anomalous Hall regime, which is robust at magnetic fields exceeding both coercive fields (Fig. 1 *C* and *D*, *Right*). Applying a magnetic field induces a topological phase transition, revealed by the appearance of 2 quantized Hall plateaus at $\sigma_{xy} = \pm e^2/h$ for the 2 magnetization directions and hysteresis that depends on the field sweep direction (Fig. 1 *E* and *F*).

To map out the evolution of the edge state pattern across the phase diagram, we plot a cross-sectional profile of the microwave response as a function of field for both sides of the hysteresis loop (Fig. 1 *G* and *H*). Our images reveal a dramatic evolution in the edge state pattern near the transition between the $N = \pm 1$ states, accompanied by a nonmonotonic change in the amplitude of the complex admittance with magnetic field. When tuned toward the coercive field, the sample enters a transition regime marked by broadening of the edge states and enhancement of the complex admittance signal. At fields beyond the transition, the sample enters into a topologically distinct $N = 0$ state (Fig. 2 *A* and *B*), whose uniform conductivity profile contrasts dramatically to the

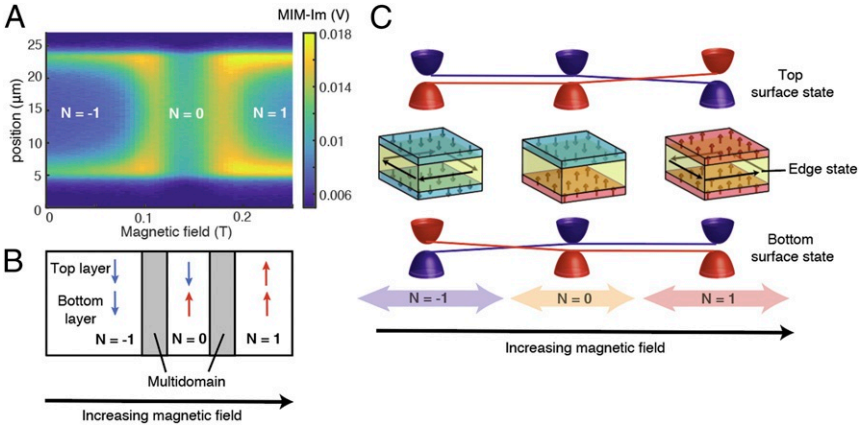

Fig. 2. Axion insulator state at the boundary between 2 quantum anomalous Hall states. (*A*) Real-space structure of the imaginary microwave conductivity evolving across the magnetic field-induced phase transitions between 3 topologically distinct states (Chern number $N = 1$ QAH state, $N = 0$ state, and $N = -1$ QAH state). (*B*) Schematic of proposed magnetic orientations of the top and bottom layers of magnetic dopants in each part of the phase diagram. (*C*) Schematic illustration of the magnetization configurations and spatial conductivity profiles for the quantum anomalous Hall state (labeled by Chern numbers $N = -1$ and 1) and the proposed axion insulator state (labeled $N = 0$) in the phase diagrams. Phase transitions correspond to band crossings that arise when the massive Dirac gap changes sign in the top or bottom surface states.

edge-dominated profile in the Chern number $N = \pm 1$ states. The boundary signal vanishes when the total magnetization of the system is near zero (Fig. 1*D*, *Left*), suggesting that the edge states in the QAH regime are topologically robust and do not have a trivial origin.

Discussion and Conclusions

Evolution of Edge State Structure across the Phase Diagram of Topological States. Fig. 2 presents a proposed phase diagram for the system. The $N = \pm 1$ transition consists of 2 steps, each separated by a multidomain region. One scenario that can give rise to this behavior features 2 magnetic dopant layers with different coercive fields, $B_{c1} < B_{c2}$. Under these circumstances, tuning the magnetic field should enable access to an expanded set of topological states associated with parallel or antiparallel magnetization configurations of the dopant layers (11, 15–17). At magnetic fields $B < B_{c1}$, both magnetizations would be aligned downward and the top and bottom surface states contribute Hall conductances of equal sign, which should yield a robust QAH state with $\sigma_{xy} = -1\ e^2/h$ (labeled $N = -1$). Because the QAH insulator would feature a magnetization that would point inward at the top surface and outward at the bottom surface, the gap of the massive Dirac dispersion (14, 24) should change sign at the sample boundaries, which gives rise to the conductive edge states that are observed in our MIM images. As the field is increased to $B = B_{c1}$, the dopant layer with the smaller coercive field should begin to flip magnetization first, leading to an initial enhancement of conductance as currents propagate along metallic domain walls in the bulk of the film.

Upon further increasing the field into the regime $B_{c1} < B < B_{c2}$, the magnetizations of the dopant layers would have opposite orientations, leading to a cancellation of the Hall conductivities on the top and bottom surface states of the topological insulator (the "axion insulator," labeled $N = 0$). Like the QAH state, the $n = 0$ phase has gapped top and bottom surfaces; unlike the QAH state, the $n = 0$ phase lacks dispersing edge modes. The dramatically different conductivity profiles associated with these topologically distinct states are evident in Fig. 2*C*. Upon increasing the magnetic field further to $B = B_{c2}$, one can flip the magnetization of the layer with the higher coercive field, leading to a phase transition into a Chern number $N = 1$ QAH state, which is stabilized when both magnetizations are aligned.

Complex Microwave Response at the Phase Transitions. To elucidate the physical origins of the microwave response at the quantum phase transitions, we use a lumped circuit model to extract quantitative information about the local dissipation and screening (*SI Appendix*). We have modeled the complex impedance $Z = 1/(i\omega C_s + 1/R_s) + 1/i\omega C$, where C_s and R_s respectively represent the local sample capacitance and resistance to ground, C is the tip-sample capacitance, and ω is the frequency. The real and imaginary MIM response can be approximated by $Re(Y)$ and $Im(Y)$, the real and imaginary parts of the admittance $Y = 1/Z$, up to a scaling factor. The experimental values of R_s and C_s, extracted from the dataset in *SI Appendix*, Fig. S1*B*, reveal a nonmonotonic evolution of bulk resistance as a function of magnetic field and an enhanced local capacitance near the phase transitions (*SI Appendix*, Fig. S3). Band crossings at the phase transitions give rise to an increased density of states, allowing the sample to more effectively screen the electric field from the tip. As such, the imaginary part of the microwave response can provide insight into gap closure at phase transitions, which we leverage to understand the nature of the $N = 0$ phase.

The Axion Insulator State. There are 2 candidate states, the axion insulator and the trivial insulator, which can give rise to

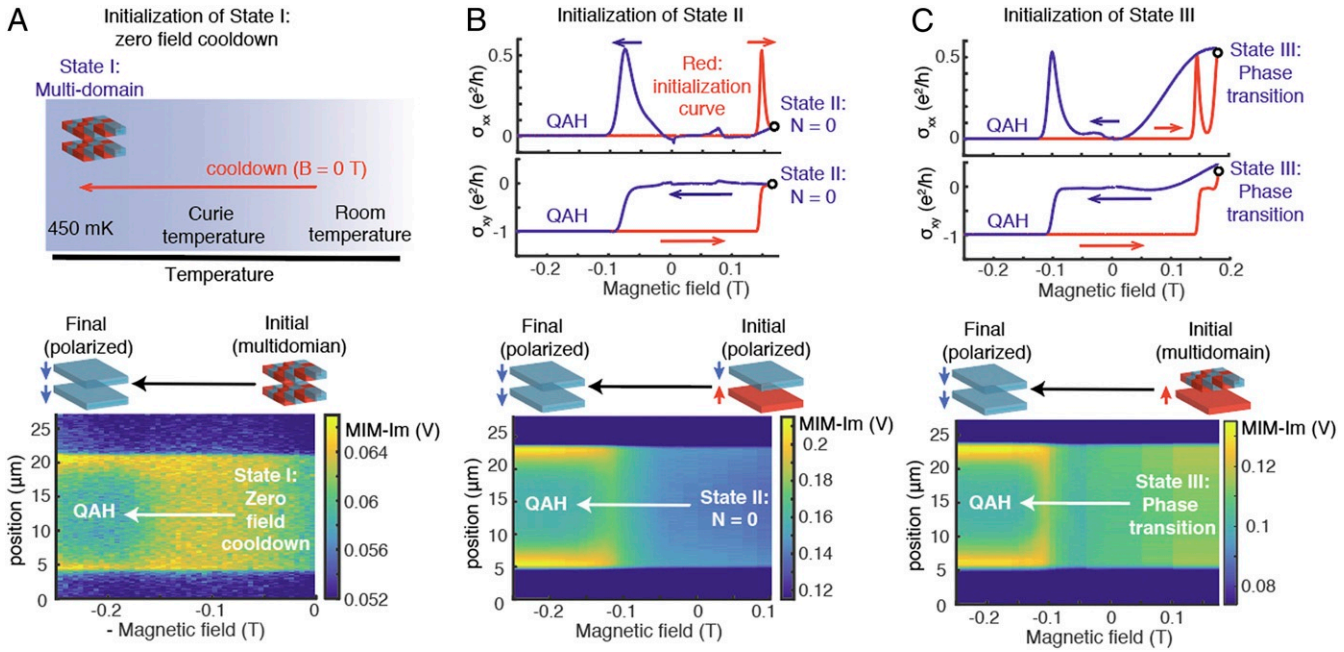

Fig. 3. Inferring the underlying magnetic domain structure of the $N = 0$ state. (*A*, *Top*) We perform measurements to infer the magnetic domain structure of various states in the phase diagram (labeled I, II, and III). We first initialize the sample in a trivial multidomain $N = 0$ state by cooling the system down at zero magnetic field. (*A*, *Bottom*) Real-space visualization of the broadened phase transition from the zero-field cooldown state into the QAH state, consistent with expected behavior for a transition from a multidomain to a single-domain magnet. (*B*, *Top*) We initialize the sample in the observed $N = 0$ state using the field sweep labeled in red. (*B*, *Bottom*) A sharp transition as a function of field, consistent with expected behavior for a transition between 2 single-domain magnets. The behavior of edge and bulk conduction across the transition matches expectations for a transition from the axion insulator state into the QAH state. (*C*, *Top*) We initialize the sample at the phase transition between the $N = 0$ and $N = 1$ states (red curve). (*C*, *Bottom*) A broad transition as a function of field, consistent with expected behavior for a transition from a multidomain to a single-domain magnet.

insulating behavior in the region of the phase diagram labeled $N = 0$. In contrast to the expected antiparallel magnetic configuration of the axion insulator state (Fig. 2 *B* and *C*), the trivial insulating state would be characterized by multidomain behavior across the phase transition between the 2 QAH states with opposite chiralities. As prior transport studies have reported identical electronic signatures for both candidate insulating states, a plateau with zero Hall conductivity, further investigation is required (4, 17, 21). To prove existence of the axion insulator, one needs to show (*i*) the top and bottom surfaces act as single magnets with opposite Hall conductivities and (*ii*) the exchange energy dominates.

Satisfying condition *i* requires identifying the underlying magnetic domain structure of the $N = 0$ state. While our technique does not directly measure the magnetization of the sample, we can deduce its magnetic properties electronically by leveraging the topological magnetoelectric effect, which defines a coupling between the electric and magnetic properties of a QAH insulator (25). Specifically, the sample can exist in 4 possible magnetic configurations, which are tunable with an external field: (*a*) Spin-up ferromagnet on both layers, the $N = 1$ state (associated with a conductivity of $\sigma_{xy} = 1e^2/h$); (*b*) spin-down ferromagnet on both layers, the $N = -1$ state ($\sigma_{xy} = -1e^2/h$); (*c*) antialigned ferromagnets on opposite layers, the axion insulator ($\sigma_{xy} = 0$); and (*d*) multidomain ($\sigma_{xy} \geq 0$).

The magnetizations of the states described in scenarios *a* and *b* can be inferred unambiguously via their electronic signatures, as shown in the transport and MIM data in Fig. 1 *E*–*H*. The magnetic structure of the $N = 0$ state, however, cannot be uniquely identified because multiple magnetic orientations could yield insulating behavior (scenarios *c* and *d*). To further distinguish between the single-domain (*c*) and multidomain (*d*) scenarios, we can reference a well-known property of magnets: A multidomain magnet undergoes a broad and continuous phase transition into a ferromagnetic state in response to an applied field, whereas a single-domain magnet undergoes a sharp, delayed transition at a finite coercive field owing to the energy barrier associated with domain nucleation.

To infer the magnetic configuration, we initialized the sample in a particular region of the phase diagram and monitored its evolution into the QAH regime as a function of magnetic field (Fig. 3). We first initialized the sample in the $N = 0$ region of the phase diagram (Fig. 3*B*, *Top*) and monitored its evolution into the QAH regime (Fig. 3*B*, *Bottom*). The microwave signal exhibits a sharp phase transition in the QAH state with an onset at a higher field. This behavior is consistent with that of a single-domain magnet, as the phase transition commences at a nonzero magnetic field because energy is required to overcome the barrier to nucleate magnetic domains. By contrast, when the sample was initialized with a random network of domains by cooling the device down at zero magnetic field (Fig. 3*A*), this multidomain state showed a broad and continuous transition into the QAH state as a function of magnetic field. As a consistency check, we initialized the system at a phase transition (Fig. 3*C*, *Top*) and observed that it also exhibited the expected multidomain broad transition into the QAH regime (Fig. 3*C*, *Bottom*).

A second way to distinguish between the 2 candidate states is by identifying whether the exchange or hybridization energy scale dominates in the $N = 0$ region of the phase diagram (condition *ii*). This question can be resolved by monitoring the magnetic fields at the 2 transition points, as described below.

For the scenario in which the hybridization dominates over the exchange energy scale, one would expect a spin-degenerate gapped parabolic band structure near zero magnetic field (trivial $N = 0$ state). The size of the energy gap between the bands is Δ_h, whose magnitude depends on the hybridization between the top and bottom surface states and therefore on the thickness of the topological insulator (*SI Appendix*). Application of a magnetic field increases the total exchange splitting between up and down spin states (labeled Δ_m) and induces a phase transition into the QAH state (Fig. 4*A*). The phase transition between the trivial $N = 0$ state and the QAH state should occur at a magnetic field corresponding to $\Delta_h = \Delta_m$, which depends on the thickness of the topological insulator film.

By contrast, the band structure evolution from the axion insulator (which is dominated by the exchange gap) into the QAH insulator should feature 2 band crossing points that coincide with the 2 coercive fields B_{c1} and B_{c2} and thus be independent of film thickness (Fig. 2*C*). Upon comparing the experimental phase diagrams from 2 films of different thicknesses, we find that the placement of the transition points does not move appreciably with field, which is qualitatively consistent with the axion insulator scenario (Fig. 4 *B* and *C*).

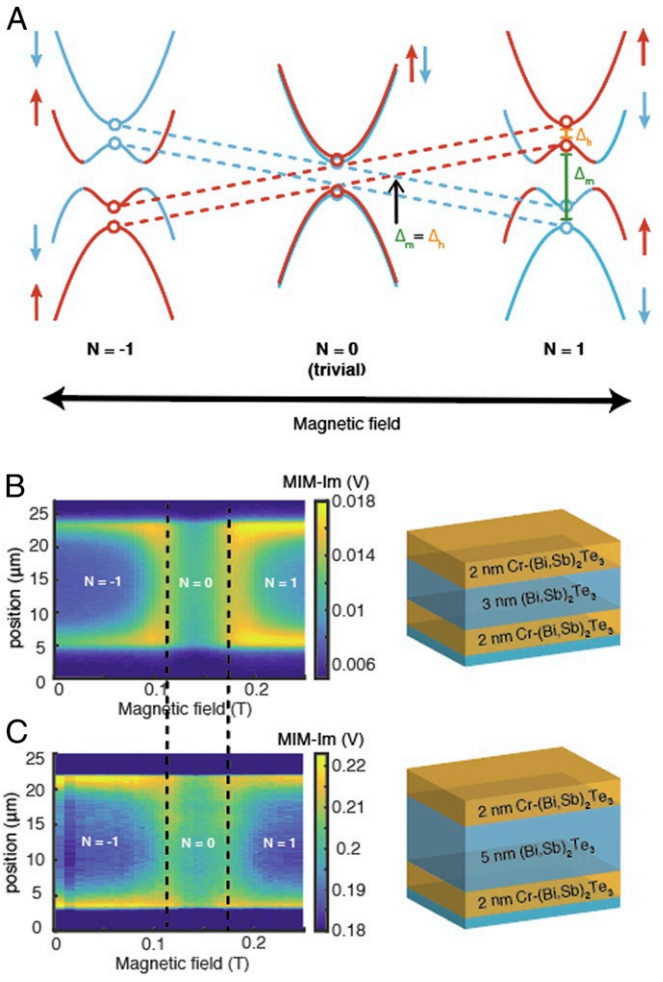

Fig. 4. Evolution of band structure with spin splitting. (*A*) Schematic: Magnetic field-induced phase transition from the trivial $N = 0$ state into the QAH state, as a function of applied magnetic field. At zero field, there is a spin degenerate gapped state, where the gap Δ_h arises from interaction between the upper and lower surface states and therefore should depend strongly on film thickness. Applying a magnetic field opens an exchange gap Δ_m, resulting in a phase transition when $\Delta_h = \Delta_m$. By contrast, the band crossings between the axion insulator and QAH states (Fig. 2*C*) should coincide with the coercive field values for the top and bottom magnetic layers. Therefore, the field strength required to induce phase transitions should be tunable with film thickness for the trivial state but not for the axion state. Our experiments probe states near zero momentum, labeled by the circles. (*B* and *C*) Phase diagrams measured in 2 films of different thickness exhibit phase transitions at similar magnetic fields, consistent with the expected behavior for the axion insulator state.

The uniform conductivity in the $N = 0$ region suggests an absence of trivial edge currents, in contrast to evidence of the contrary in other systems, such as quantum spin Hall candidate InAs (26). Due to the purely topological nature of the observed edge states, this system constitutes an attractive platform to visualize Majorana modes and harness them for topological quantum computing applications in the future (27, 28).

Materials and Methods

Magnetic topological insulator films were grown by molecular beam epitaxy (MBE) on semi-insulating InP(111) substrates using the same procedures as described in ref. 21. The 3-nm-thick AlO_x capping layer was deposited by the atomic layer deposition (ALD) system immediately after the removal from the MBE chamber. The Hall bar (400 μm width) and strip (20 μm width) devices were defined by photolithography and Ar-ion milling, followed by chemical wet etching with an HCl-H_3PO_4 mixture for removing the damaged side edge and substrate surface. For ohmic contact electrodes, 5-nm-thick Ti and subsequent 45-nm-thick Au were deposited by electron beam evaporation.

ACKNOWLEDGMENTS. We thank B. Lian, A. MacDonald, M. Masir, D. H. Lee, M. Kawasaki, A. Tsukazaki, and R. Yoshimi for their collaboration on the sample preparation and discussions. This work was partly supported by Japan Science and Technology Agency Core Research for Evolutional Science and Technology (JPMJCR16F1). Microwave impedance microscopy measurements at Stanford University were supported by the Gordon and Betty Moore Foundation's Emergent Phenomena in Quantum Systems initiative through Grant GBMF4546 (Z.-X.S.) and by the National Science Foundation through Grant DMR-1305731. Device transport measurements at Stanford University were supported by the US Department of Energy, Office of Science, Basic Energy Sciences, Materials Sciences and Engineering Division, under Contract DE-AC02-76SF00515. M.A. acknowledges support from the Karel Urbanek Fellowship in Applied Physics at Stanford University.

1. C. Z. Chang *et al.*, Experimental observation of the quantum anomalous Hall effect in a magnetic topological insulator. *Science* **340**, 167–170 (2013).
2. J. G. Checkelsky, J. Ye, Y. Onose, Y. Iwasa, Y. Tokura, Dirac-fermion-mediated ferromagnetism in a topological insulator. *Nat. Phys.* **8**, 729–733 (2012).
3. J. G. Checkelsky *et al.*, Trajectory of the anomalous Hall effect towards the quantized state in a ferromagnetic topological insulator. *Nat. Phys.* **10**, 731–736 (2014).
4. X. Kou *et al.*, Scale-invariant quantum anomalous Hall effect in magnetic topological insulators beyond the two-dimensional limit. *Phys. Rev. Lett.* **113**, 137201 (2014).
5. C. Z. Zhang *et al.*, High-precision realization of robust quantum anomalous Hall state in a hard ferromagnetic topological insulator. *Nat. Mater.* **14**, 473–477 (2015).
6. A. J. Bestwick *et al.*, Precise quantization of the anomalous Hall effect near zero magnetic field. *Phys. Rev. Lett.* **114**, 187201 (2015).
7. M. Liu *et al.*, Large discrete jumps observed in the transition between Chern states in a ferromagnetic topological insulator. *Sci. Adv.* **2**, e1600167 (2016).
8. S. Grauer *et al.*, Scaling of the quantum anomalous Hall effect as an indicator of axion electrodynamics. *Phys. Rev. Lett.* **118**, 246801 (2017).
9. X. L. Qi, T. L. Hughes, S. C. Zhang, Topological field theory of time-reversal invariant insulators. *Phys. Rev. B* **78**, 195424 (2008).
10. R. Yu *et al.*, Quantized anomalous Hall effect in magnetic topological insulators. *Science* **329**, 61–64 (2010).
11. C. X. Liu, S. C. Zhang, X. L. Qi, The quantum anomalous Hall effect: Theory and experiment. *Annu. Rev. Condens. Matter Phys.* **7**, 301–321 (2016).
12. J. Wang, B. Lian, S. C. Zhang, Universal scaling of the quantum anomalous Hall plateau transition. *Phys. Rev. B* **89**, 085106 (2014).
13. F. D. M. Haldane, Nobel lecture: Topological quantum matter. *Rev. Mod. Phys.* **89**, 040509 (2017).
14. Y. L. Chen *et al.*, Massive Dirac fermion on the surface of a magnetically doped topological insulator. *Science* **329**, 659–662 (2010).
15. J. Wang, B. Lian, X. L. Qi, S. C. Zhang, Quantized topological magnetoelectric effect of the zero-plateau quantum anomalous Hall state. *Phys. Rev. B* **92**, 081107 (2015).
16. T. Morimoto, A. Furusaki, N. Nagaosa, Topological magnetoelectric effects in thin films of topological insulators. *Phys. Rev. B* **92**, 085113 (2015).
17. M. Mogi *et al.*, A magnetic heterostructure of topological insulators as a candidate for an axion insulator. *Nat. Mater.* **16**, 516–521 (2017).
18. M. Mogi *et al.*, Tailoring tricolor structure of magnetic topological insulator for robust axion insulator. *Sci. Adv.* **3**, eaao1669 (2017).
19. D. Xiao *et al.*, Realization of the axion insulator state in quantum anomalous Hall sandwich heterostructures. *Phys. Rev. Lett.* **120**, 056801 (2017).
20. E. O. Lachman *et al.*, Visualization of superparamagnetic dynamics in magnetic topological insulators. *Sci. Adv.* **1**, e1500740 (2015).
21. M. Mogi *et al.*, Magnetic modulation doping in topological insulators toward higher-temperature quantum anomalous Hall effect. *Appl. Phys. Lett.* **107**, 182401 (2015).
22. W. Kundhikanjana, K. Lai, M. A. Kelly, Z. X. Shen, Cryogenic microwave imaging of metal-insulator transition in doped silicon. *Rev. Sci. Instrum.* **82**, 033705 (2011).
23. Y. Cui, E. Y. Ma, Z. X. Shen, Quartz tuning fork based microwave impedance microscopy. *Rev. Sci. Instrum.* **87**, 063711 (2016).
24. I. Lee *et al.*, Imaging Dirac-mass disorder from magnetic dopant atoms in the ferromagnetic topological insulator crx(bi0.1sb0.9)2-xte3. *Proc. Natl. Acad. Sci. U.S.A.* **112**, 1316–1321 (2015).
25. X. L. Qi, R. Li, J. Zang, S. C. Zhang, Inducing a magnetic monopole with topological surface states. *Science* **323**, 1184–1187 (2009).
26. F. Nichele *et al.*, Edge transport in the trivial phase of InAs/GaSb. *New J. Phys.* **18**, 083005 (2016).
27. Q. L. He *et al.*, Chiral Majorana fermion modes in a quantum anomalous Hall insulator–superconductor structure. *Science* **357**, 294–299 (2017).
28. J. Wang, Q. Zhou, B. Lian, S. C. Zhang, Chiral topological superconductor and half-integer conductance plateau from quantum anomalous Hall plateau transition. *Phys. Rev. B* **92**, 064520 (2015).